PAPER

Check for updates

A novel flexible egtazic acid/cerium-based metal organic framework as a potent catalyst for the synthesis of benzochromenoquinolinones and triazolopyrimidines

Ghazale Almasi, Davood Habibi, (ID) * Hosein Khodakarami and Masoumeh Beiranvand

The sponge-like structures of metal–organic frameworks (MOFs) are ideal platforms for various applications due to their structural diversity and adjustability, which allow for targeted design and synthesis. In recent years, substantial advances in the field of MOFs have been achieved, especially those containing aromatic ligands. Although there are several publications related to aliphatic ligands, the aliphatic MOFs developed are rather limited. Herein, a novel cerium-based flexible MOF (Ce-MOF-EGTA) constructed from an aliphatic tetratopic EGTA linker is reported. The framework exhibits high crystallinity, permanent porosity, and thermal stability up to 360 °C, as confirmed by FT-IR, EDX, elemental mapping, FESEM, XRD, TGA/DTA, and BET/BJH analyses. The presented flexible MOF is highly crystalline in nature and is stable up to 360 °C. Owing to the combination of intrinsic framework flexibility and accessible Ce Lewis acid sites, Ce-MOF-EGTA functions as an efficient heterogeneous catalyst for the synthesis of 6H-chromeno [4,3-b]quinolin-6-ones and 1,2,4-triazolo[4,3-a]pyrimidines, providing high yields under mild conditions with short reaction times. The catalyst demonstrates excellent stability and reusability over five consecutive cycles, with negligible cerium leaching and preservation of the original framework structure.

Introduction

MOFs are self-assembled materials formed by covalent bonds between metal ions or clusters and organic linkers. MOFs have attracted much attention from researchers over the past few decades due to their properties, such as various synthesis methods, high porosity, high surface area, spatially separated catalytic active sites, adjustable pore size and void volume, ordered crystalline shapes, structural, high thermal and chemical stabilities, and so on.[1–6]

MOFs have wide applications in various fields such as catalysts, photocatalysis, photo-luminescence, sorption and separation, water remediation, drug storage and delivery, imaging, and sensors.[7–12] The catalytic behavior of MOFs arises from both their metal centers and organic linkers. Broadly, three different types of active sites in MOFs act as reaction chambers:

(i) coordinatively unsaturated metal centers that coordinate with the substrate and catalyze the reaction,

(ii) the second type of site involves encapsulation or incorporation of active catalytic species inside the pores of MOF for synergistically enhanced catalysis, and

(iii) Functionalized ligands present in the framework to initiate the reaction.[13]

In general, most MOFs are based on aromatic carboxylates[14,15] and *N*-donor ligands,[16] which possess their structural rigidity and, therefore, allow a more straightforward design and predictable functionalization of the polymeric lattice, but an important advantage of MOFs is the variety of metal ions and organic ligands used in them.

According to the theories of Susumu Kitagawa and the type of ligand used in the synthesis of the MOFs based on the intactness of the framework upon interaction with the guest molecule, there are four types of MOFs (Fig. 1):

(i) in which the framework collapses upon desorption of the guest molecule, (ii) the framework remains intact during the removal of a guest molecule, (iii) a flexible type framework adjusts its shape by changing pore volume on guest uptake and restores its size upon guest removal, and (iv) structures that are associated with post-synthetic modifications.[17,18]

Many MOFs have been built based on aromatic or rigid ligands, such as 2-amino-terephthalic acid, benzene dicarboxylic acid, 1,3,5-benzene-tricarboxylic acid, 2-methylimidazole, biphenyl-4,4′-dicarboxylic acid, 2-(5-pyridin-4-yl-2*H*-[1,2,4] triazol-3-yl)-pyrimidine and so on.[19–24]

The synthesis of MOFs using aliphatic ligands is an emerging field that has attracted the attention of researchers

Department of Organic Chemistry, Faculty of Chemistry and Petroleum Sciences, Bu-Ali Sina University, Hamedan, Iran. E-mail: davood.habibi@gmail.com; dhabibi@basu. ac.ir; Fax: +98 81 31408025; Tel: +98 81 31406070
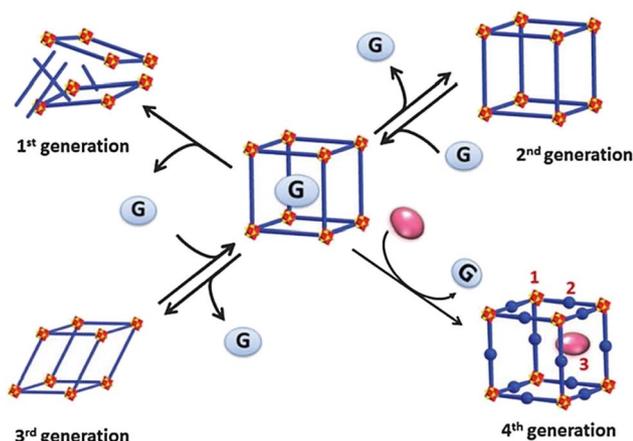
Fig. 1   Types of MOFs based on Susumu Kitagawa's theory.

due to its features, such as increased structural freedom, non-polar core, low light absorption, high hydrophobicity, controllable dynamics, and application in medicine. It has many applications in gas absorption, heterogeneous catalysis, and proton conduction.[25–28] The presence of a saturated hydrocarbon core is a promising trend for the synthesis of biocompatible and biostable MOFs compared to MOFs with aromatic ligands.

The use of aliphatic ligands results in flexible frameworks, which are capable of responding to external stimuli such as temperature, pressure, light, electric field, inclusion of chemicals, etc., but they are also crystalline and can reversibly change their channels while maintaining their topology. These FL-MOFs are often associated with reversible transformations between two or more states related to expansion and contraction. This phenomenon is often known as the breathing effect,[29,30] sponge-like effect,[31–33] or accordion effect.[34]

So far, various MOFs have been constructed using aliphatic ligands such as cyclohexane-1,2,4,5-tetracarboxylic acid, alkane dioic acids, glutamic acid, mesaconic acid, 1,4-cyclohexane dicarboxylic acid, and 1,4-diazabicyclo[2,2,2]octane (DABCO) (Fig. 2).[35–41]

Chromeno[4,3-b]quinolines consist of two fused chromene and quinoline rings, which have wide applications in various fields such as biology, medicine, physics, and electronics.[42–46]

Triazolopyrimidines are also an attractive class of N-heterocycles because these compounds are widely used in the pharmaceutical and agricultural industries and have significant potential in a wide range of biological activities, such as antibacterial, antifungal, antiviral, anticancer, anti-inflammatory, analgesic, and central nervous system activators.[47–53]

In this work, a new FL-MOF (Ce-MOF-EGTA) was synthesized from the reaction of Ce(IV) ammonium nitrate {CAN = $(NH_4)_2[Ce(NO_3)_6]$} with an aliphatic ligand, namely ethylene glycol-bis(β-aminoethyl ether)-N,N,N′,N′-tetraacetic acid (EGTA), also known as egtazic acid. EGTA is an aminopoly-carboxylic tetratopic acid ligand, which can bind to metal ions as a chelating agent. Then, the catalytic potential of Ce-MOF-EGTA was explored as a heterogeneous catalyst for the synthesis of benzochromenoquinolines **1(a–g)** and triazolopyrimidines **2(a–g)**. The Ce-MOF-EGTA was synthesized in a simple, one-step method and showed high catalyst activity. Compared to other catalysts used in the synthesis of benzochromenoquinolines and triazolopyrimidines, Ce-MOF-EGTA produced products with higher yields and a more convenient purification method.

Experimental

General

All the commercial reagents were provided by the foreign chemical companies and used as received. The reaction progression and purity of the prepared compounds were monitored by thin-layer chromatography (TLC) performed with silica gel 60 F 254 plates. Fourier transform infrared (FT-IR) spectra were recorded on a PerkinElmer Spectrum Version 10.02.00 employing KBr pellets. The ^1H NMR (250 and 400 MHz) and ^{13}C NMR (62.5 and 125 MHz) spectra were taken on a Bruker spectrometer (δ in ppm) using DMSO-d_6 as a solvent with chemical shifts measured relative to TMS as the internal standard. Melting points were taken with a BUCHI 510 melting point apparatus. Elemental analysis was performed using a MIRA II analyzer. The field-emission scanning electron microscopy (FESEM) images were recorded using a MIRA III analyzer. The X-ray diffraction (XRD) measurements were carried out with an XRD Philips PW1730. Thermo-gravimetric differential thermal analysis (TGA-DTA) was done using an SDT-Q600 device.

General strategy for the synthesis of Ce-MOF-EGTA

Ce-MOF-EGTA was synthesized according to the previously established solvothermal procedure by Wang and Li.[54] Briefly, CAN (0.0437 mmol) and EGTA (0.0368 mmol) were stirred in a mixed solvent (DMF/HCOOH, 1:2, 7.5 mL) for 10 min at room temperature. The mixture was then placed in a Teflon reactor and placed in an oven at 120 °C for 72 h. The mixture was then slowly cooled to room temperature, centrifuged, washed with DMF and dichloromethane, and dried in vacuo at 100 °C for 24 h. The obtained white Ce-MOF-EGTA was then characterized
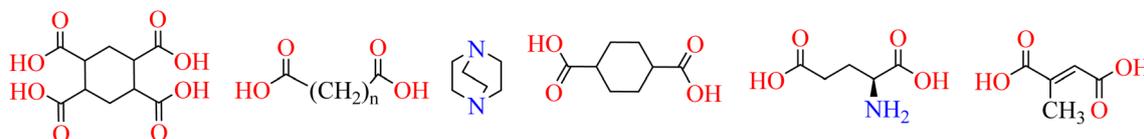

Fig. 2   Some aliphatic or alicyclic ligands.

by FT-IR, EDX, Elemental mapping, XRD, FESEM, TGA/DTA, and BET/BJH analyses (Fig. 3).

General procedure for the synthesis of 1(a–g) and 2(a–g) by Ce-MOF-EGTA

For the synthesis of **1(a–g)**, 4-hydroxycumarine (0.1621 g, 1.0 mmol), 1-naphthylamine (0.1431 g, 1.0 mmol), aromatic aldehydes (1 mmol), and Ce-MOF-EGTA (20 mg) were mixed and stirred at 80 °C under solvent-free conditions. The progress of the reaction was pursued using TLC (n-hexane/EtOAc, 7 : 3). At the end, the resultant solid was dissolved in DMF (10 mL) and centrifuged to separate the catalyst. Then, the crude product was then purified using ethanol and acetone and characterized by FT-IR, NMR, and melting point analysis. Also, for the synthesis of **2(a–g)**, 3-amino-1,2,4-triazole (84 mg, 1.0 mmol), malononitrile (66 mg, 1.0 mmol), aromatic aldehydes (1.0 mmol), and Ce-MOF-EGTA (20 mg) were mixed at 110 °C under solvent-free conditions for appropriate times, and the reaction progress was monitored by TLC (n-hexane/EtOAc, 5 : 5). After completion of the reaction, the solid was dissolved in DMF (10 mL) and centrifuged to separate the catalyst. The product was purified using ethanol and ethyl acetate, and characterized by FT-IR, NMR, and melting point analyses.

Results and discussion

Characterization of Ce-MOF-EGTA

The novel MOF was characterized by several techniques, including FT-IR, XRD, EDX, elemental mapping, FESEM, TGA/DTA, and BET/BJH.

Characterization by FT-IR spectroscopy

The FT-IR spectra of EGTA and Ce-MOF-EGTA are demonstrated in Fig. 4. The FT-IR spectrum of the EGTA ligand shows the peaks at 3436, 1739, 1134, and 1100 cm^{-1}, which are related to the O–H, C=O, C–N, and C–O. The FT-IR spectrum of Ce-MOF-EGTA shows distinct absorption bands at 2912, 1601, 1574, 1428, 1404, 1357 and 778 cm^{-1} for C–H, C=O, CH_2, C–N, C–O, C–C and Ce–O, respectively, as well as a sharp decrease in O–H absorption, carbonyl peak shift and the presence of a new peak at 778 cm^{-1} corresponding to Ce–O, confirms the successful synthesis of the catalyst.
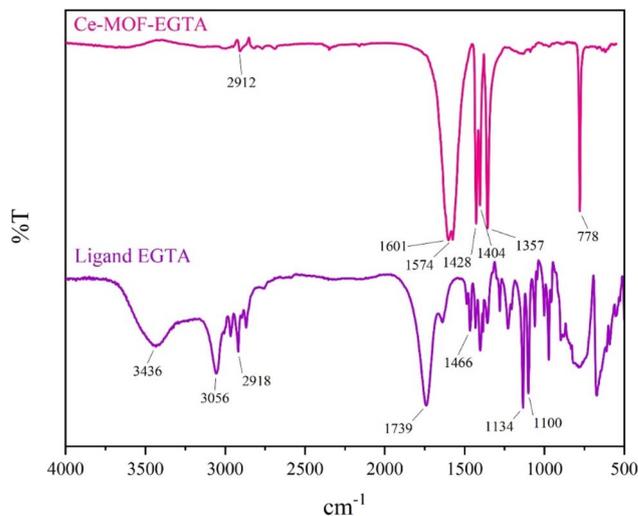

Fig. 4 The FT-IR spectra of the EGTA ligand, and Ce-MOF-EGTA.

Characterization by EDX and elemental mapping analysis

The existence of Ce, O, C, and N elements in the chemical composition of Ce-MOF-EGTA was confirmed by EDX analysis. In addition, EDX mappings represent the homogeneous distribution of all elements in the framework (Fig. 5).

Characterization by the FESEM analysis

The morphology of the synthesized framework was examined using field emission scanning electron microscopy (FESEM). The particle size distribution histogram was also examined. FESEM images showed rod-like particles with a uniform size and homogeneous particle distribution for Ce-MOF-EGTA. As can be observed, the size of the rod-like particles is approximately 0.345–0.770 μm (Fig. 6).

Characterization by XRD analysis

The XRD analysis confirms the highly crystalline nature of the newly synthesized framework and EGTA ligand (Fig. 7) with the characteristic peaks observed at 2θ = 18.7, 25.8, 31.2, 35.8, 43.5, 47.1, 50, 53.6, 56.5, 59.7, 62.1 and 65.1. For comparison, the free EGTA ligand shows peaks at 2θ = 13.7, 15.5, 16.4, 17.1, 20.4, 21.1, 23.5, 24.8, 27.1, 27.8, 28.6, 3., 31.4, 32.1, 34.7 and 41.8, confirming its incorporation into the MOF framework.
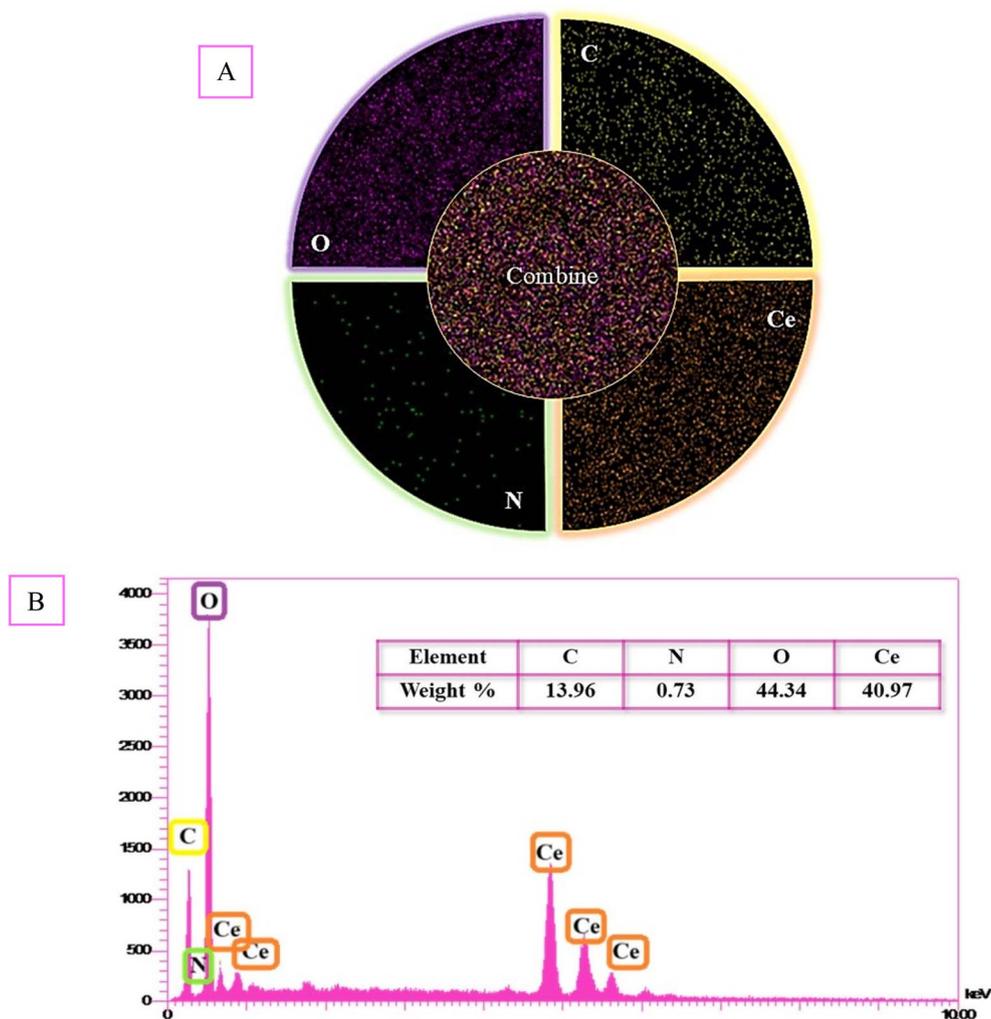

Fig. 3 Synthesis of Ce-MOF-EGTA.

Fig. 5   EDX (A) and elemental mapping (B) analysis.

Characterization by BET/BJH

The specific surface area of Ce-MOF-EGTA was characterized using the N_2 adsorption–desorption analysis. The results are presented in Fig. 8, and the corresponding detailed parameters are listed in Table 1.

As observed from the BET analysis results, the surface area, pore volume (V_m), and total pore volume ($cm^3 g^{-1}$) of Ce-MOF-EGTA are 5.1 $m^2 g^{-1}$, 1.18 $cm^3 g^{-1}$, and 0.014 $cm^3 g^{-1}$, respectively (Fig. 8a). Additionally, the obtained BJH adsorption indicated that the pore size of Ce-MOF-EGTA is approximately 1.22 nm (Fig. 8b).

The BET surface areas and gas uptake capacities of most FL-MOFs are relatively low compared with the estimations by computational studies. This phenomenon can be reasonably explained by channel collapse (or partial collapse) upon solvent removal or channel blockage on account of partial solvent retention. On the one hand, FL-MOFs have been found particularly susceptible to incomplete activation or loss of porosity owing to the flexibility of the bridging organic linkers, which can hardly sustain the frameworks.[25] In general, as the length of the linking chain increases, the surface area and pore volume of the framework decrease.[27] Despite the low BET values, the catalytic activity of Ce-MOF-EGTA can be affected by external surfaces and partially open pores. In addition, the measured mean pore diameter in the mesoporous range suggests that the framework still contains open channels sufficient for substrate diffusion.

Characterization by TGA-DTA

Thermogravimetric analysis (TGA-DTA) was conducted under an air flow and a temperature increase rate of 10 °C min^{-1} to investigate the thermal behavior of the Ce-MOF-EGTA. The TGA-DTA curves of Ce-MOF-EGTA exhibit a two-step weight loss upon heating in the temperature range of 25 to 800 °C under airflow conditions (Fig. 9).

The first weight loss between 50 and 110 °C is attributed to the loss of solvent molecules from the pores and also to molecules coordinated within the cage of the MOF. The second weight loss, occurring at 320 to 360 °C, is probably due to the collapse of the MOF structure and the loss of the organic linkers. Moreover, approximately 60% of the initial mass remains at 800 °C.
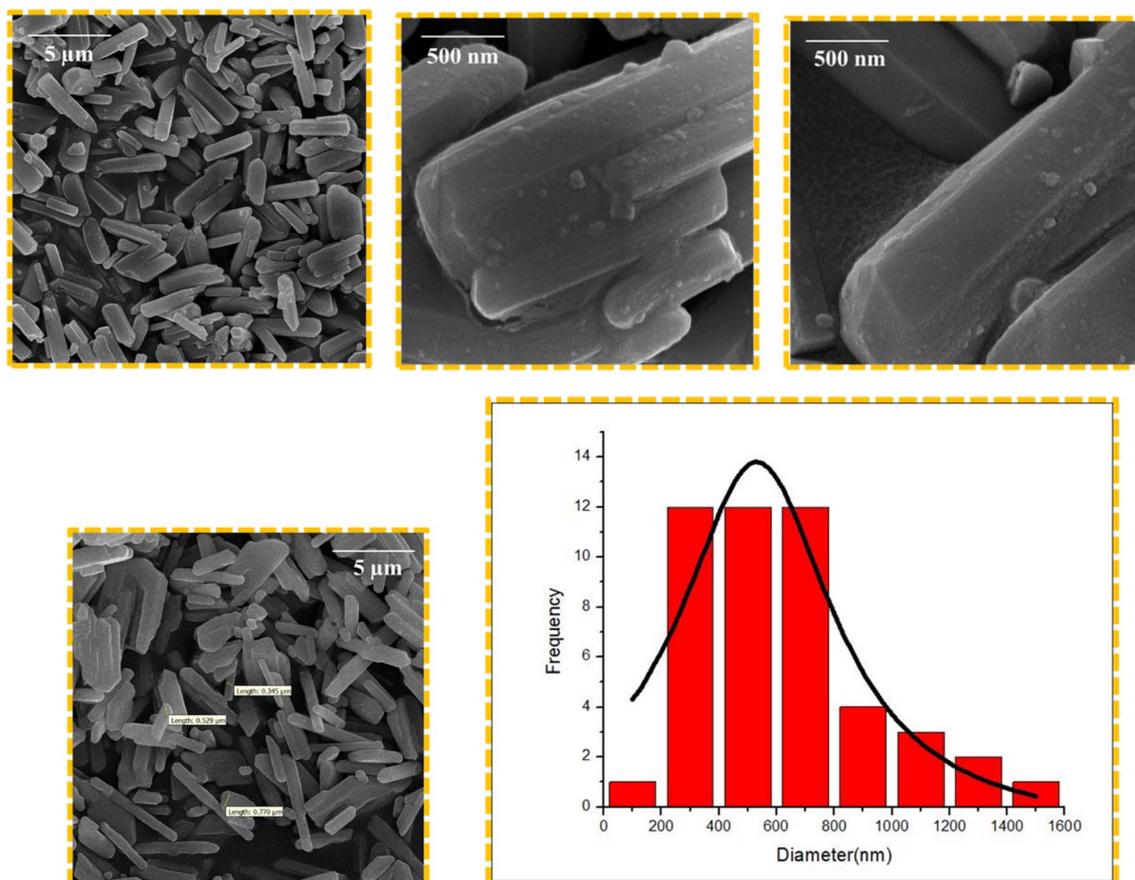
Fig. 6 (A) FESEM image of Ce-MOF-EGTA, and (B) particle size distribution histogram of Ce-MOF-EGTA.
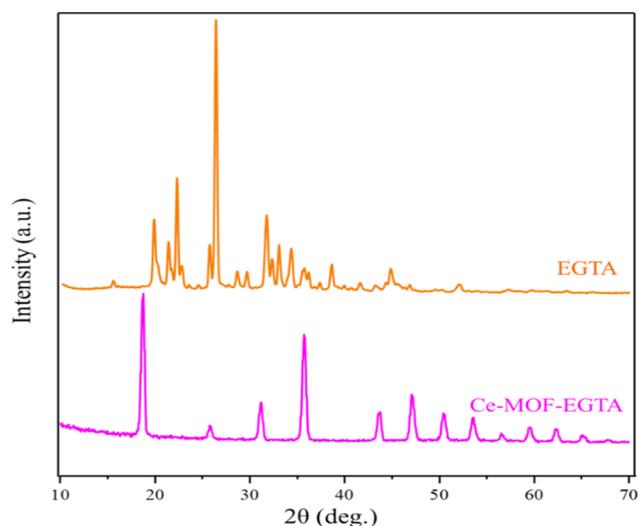

Fig. 7 The XRD pattern of Ce-MOF-EGTA.

Catalytic studies

Optimization of the reaction conditions. After characterizing the FL-MOF catalyst, its catalytic activity was evaluated in the synthesis of **1(a–g)** and **2(a–g)**. Here, you can see the effect of catalyst amount, temperature, reaction time, and solvent.

Optimization of the reaction conditions for the synthesis of 1(a–g) and 2(a–g). For the synthesis of **1(a–g)**, synthesis of **1b** (7-(2-methoxyphenyl)-7,14-dihydro-6*H*-benzo[*h*]chromeno[4,3-*b*] quinolin-6-one) by Ce-MOF-EGTA from the reaction of 4-hydroxycoumarin, 1-naphthylamine, and 2-methoxy-benzaldehyde was chosen as a model reaction. The best condition was found to be the 1 : 1 : 1 molar ratio of starting materials with 20 mg of Ce-MOF-EGTA at 80 °C in solvent-free conditions (entry 2, Table 2).

With increasing the reaction time and catalyst amount, lower yields were observed, which is likely due to the increase the side reactions. In general, the polar solvents showed more efficacy than non-polar solvents; however, they gave lower yields compared to the solvent-free conditions.

In addition, to confirm the role of Ce-MOF-EGTA in the synthesis of **1(a–g)**, three separate similar reactions were carried out in the presence of CAN, EGTA, and a mixture of CAN + EGTA as catalysts, and it was observed that the corresponding yields of **1b** decreased to 58%, 47%, and 62%, respectively.

For the synthesis of **2(a–g)**, synthesis of **2b** (5-amino-7-(2-methoxyphenyl)-7,8-dihydro-[1,2,4]triazolo[4,3-*a*] pyrimidine-6-carbonitrile) by Ce-MOF-EGTA from the reaction of 3-amino-1,2,4-triazole, malononitrile, and 2-methoxy benzaldehyde was chosen as a model reaction. The best condition was found to be the 1 : 1 : 1 molar ratio of starting materials with 20 mg of
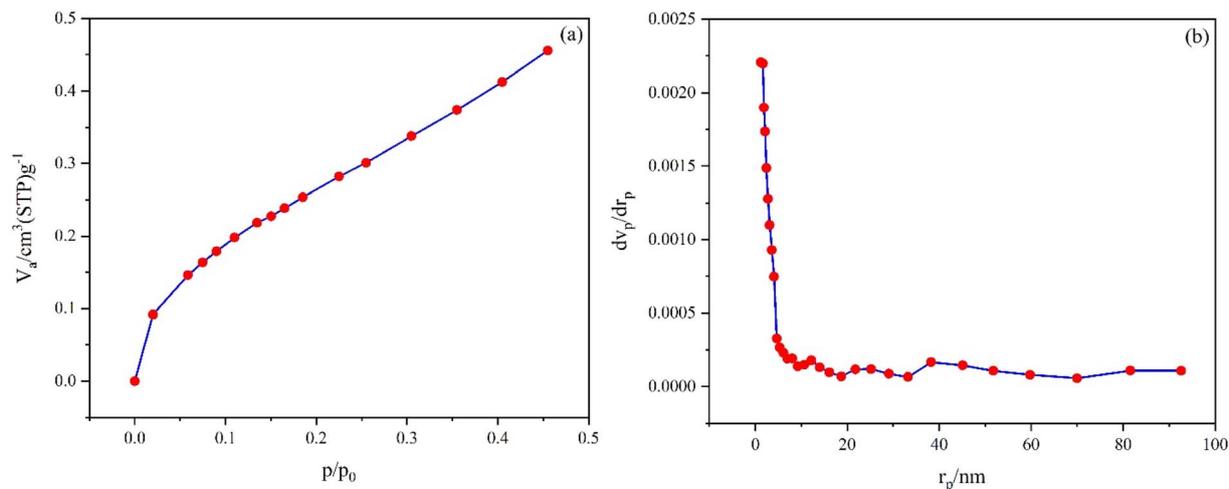
Fig. 8 The N$_2$ adsorption–desorption analysis.

Table 1 The obtained results from the BET measurements

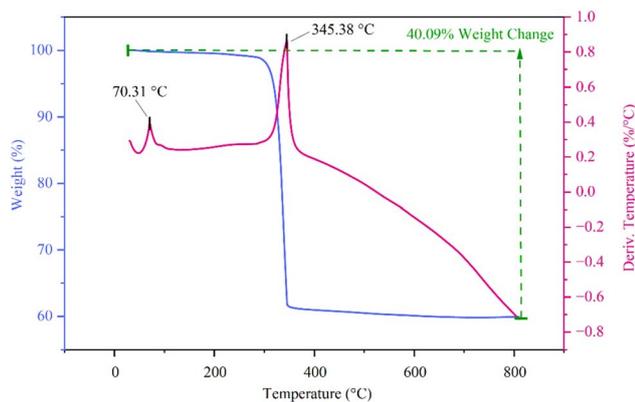| Entry	Parameter	Ce-MOF-EGTA
1	a_s (cm^3 g^{-1})	5.15
2	V_m (cm^3 g^{-1})	1.18
3	Total pore volume (cm^3 g^{-1})	0.014
4	Mean pore diameter (nm)	11.27

Fig. 9 TGA/DTA curve of Ce-MOF-EGTA.

Ce-MOF-EGTA at 110 °C in solvent-free conditions (entry 2, Table 3).

With increasing the reaction time and catalyst amount, lower yields were observed, which is likely due to the increase in the side reactions. In general, the polar solvents showed more efficacy than non-polar solvents; however, they gave lower yields compared to the solvent-free conditions.

In addition, to confirm the role of Ce-MOF-EGTA in the synthesis of 2(a–g), three separate similar reactions were carried out in the presence of CAN, EGTA, and a mixture of CAN + EGTA as catalysts, and it was observed that the corresponding yields of 2b decreased to 61%, 53%, and 75%, respectively.

Synthesis of 1(a–g) (Table 4) and 2(a–g) (Table 4). Based on the results obtained from the model reaction (1b), diverse 1(a–g) were synthesized.

Based on the results obtained from the model reaction (2b), diverse 2(a–g) were synthesized.

**Spectral data for 1(a–g) and 2(a–g)**

7-(Naphthalen-1-yl)-7,14-dihydro-6H-benzo[h]chromeno[4,3-b] quinolin-6-one (1a). Cream solid, M.P. >300 °C, IR (KBr, cm^{-1}): 3369 (NH), 3040 (C–H aromatic), 1663 (C=O), 1621 (NH bend), 1473 (C=C aromatic) and 1267 (C–O). ^{1}H NMR (250 MHz, DMSO-d$_6$) δ = 9.46 (s, 1H, NH), 8.78 (d, J = 8.6 Hz, 1H, H aromatic), 8.61 (t, J = 10.1 Hz, 2H, H aromatic), 7.87 (d, J = 8.0 Hz, 1H, H aromatic), 7.76 (d, J = 7.8 Hz, 1H, H aromatic), 7.61 (q, J = 7.5 Hz, 4H, H aromatic), 7.51 (d, J = 7.4 Hz, 3H, H aromatic), 7.38 (d, J = 8.6 Hz, 4H, H aromatic), 7.15 (d, J = 8.3 Hz, 1H, H aromatic), 6.25 (s, 1H, H aliphatic). ^{13}C NMR (62.5 MHz, DMSO-d$_6$) δ = 152.7 (C=O), 145.5, 144.5, 133.8, 133.0, 132.3, 130.8, 129.8, 128.6, 126.8, 126.4, 124.5, 124.1, 123.3, 122.4, 121.8, 117.2, 114.0, 100.1 (C aromatic), 37.0 (C aliphatic).

7-(2-Methoxyphenyl)-7,14-dihydro-6H-benzo[h]chromeno[4,3-b] quinolin-6-one (1b). Yellow solid, M.P. >300 °C, IR (KBr, cm^{-1}): 3343 (NH), 3060 (C–H aromatic), 1665 (C=O), 1621 (NH bend), 1471 (C=C aromatic) and 1241 (C–O). ^{1}H NMR (250 MHz, DMSO-d$_6$) δ = 9.37 (s, 1H, NH), 8.57 (t, J = 7.7 Hz, 2H, H aromatic), 7.80 (d, J = 8.0 Hz, 1H, H aromatic), 7.60 (dd, J = 13.8, 7.7 Hz, 2H, H aromatic), 7.49 (dt, J = 8.4, 4.3 Hz, 3H, H aromatic), 7.37 (d, J = 8.4 Hz, 2H, H aromatic), 7.08 (t, J = 8.7 Hz, 2H, H aromatic), 6.94 (d, J = 8.0 Hz, 1H, H aromatic), 6.74 (t, J = 7.3 Hz, 1H, H aromatic), 5.76 (d, J = 2.6 Hz, 1H, H aliphatic) 3.83 (s, 3H, OCH$_3$). ^{13}C NMR (62.5 MHz, DMSO-d$_6$) δ = 160.7 (C=O), 156.1, 152.8, 145.2, 136.0, 132.9, 132.2, 130.2, 129.0, 128.5, 128.2, 127.3, 126.3, 124.1, 123.2, 122.2, 121.4, 121.2, 117.1, 114.1, 112.1, 98.5 (C aromatic), 56.2 (OCH$_3$), 35.6 (C aliphatic).

7-(4-Isopropylphenyl)-7,14-dihydro-6H-benzo[h]chromeno[4,3-b] quinolin-6-one (1c). Yellow solid, M.P. 305–307 °C, IR (KBr, cm^{-1}): 3463 (NH), 3044 (C–H aromatic), 2954 (C–H

RSC Advances

Table 2 Screening the reaction parameters for the synthesis of **1b** by Ce-MOF-EGTA
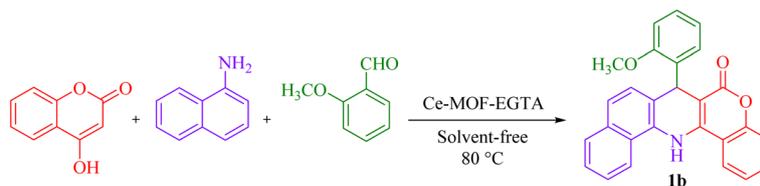
Entry	Condition	Catal. amount (mg)	Time (min)	Yield (%)
1	Solvent-free, 70 °C	20	10	86
2	**Solvent-free, 80°C**	**20**	**10**	**97**
3	Solvent-free, 100 °C	20	10	83
4	Solvent-free, 110 °C	20	10	75
5	Solvent-free, 80 °C	10	10	80
6	Solvent-free, 80 °C	30	10	78
7	Solvent-free, 80 °C	20	20	70
8	Solvent-free, 80 °C	20	30	65
9	Solvent-free, 80 °C	—	30	12
10	DMF, 80 °C	20	10	63
11	EtOH, reflux	20	10	75
12	CH₃CN, reflux	20	10	68
13	THF, reflux	20	10	45
14	Toluene, reflux	20	10	23
15	*n*-Hexane, reflux	20	10	15
16	H₂O, reflux	20	10	20

aliphatic), 1702 (C=O), 1639 (NH bend), 1473 (C=C aromatic) and 1267 (C–O). ^{1}H NMR (250 MHz, DMSO-d$_6$) δ = 9.49 (s, 1H, NH), 8.59 (dd, J = 16.6, 8.2 Hz, 2H, H aromatic), 7.85 (d, J = 8.0 Hz, 2H, H aromatic), 7.57 (ddt, J = 25.4, 18.9, 8.3 Hz, 6H, H aromatic), 7.36 (t, J = 7.9 Hz, 2H, H aromatic), 7.18 (d, J = 7.8 Hz, 2H, H aromatic), 7.05 (d, J = 7.6 Hz, 2H, H aromatic), 5.32 (s, 1H, H aliphatic), 2.73 (s, 1H, –CH$_2$–), 1.08 (d, J = 6.9 Hz,

6H, isopropyl). ^{13}C NMR (62.5 MHz, DMSO-d$_6$) δ = 160.9 (C=O), 156.7, 154.1, 152.7, 147.6, 147.0, 144.9, 139.4, 134.9, 132.3, 130.5, 128.6, 127.6, 126.8, 126.6, 124.4, 123.9, 121.7, 117.2 (C aromatic), 33.4 (C aliphatic), 24.2 (isopropyl).

7-(3-Hydroxyphenyl)-7,14-dihydro-6H-benzo[h]chromeno[4,3-b] quinolin-6-one (1d). Yellow solid, M.P. 336–339 °C, IR (KBr, cm^{-1}): 3442 (NH), 3275 (OH), 3066 (C–H aromatic), 2903

Table 3 Optimization of the reaction parameters for the synthesis of **2b** by Ce-MOF-EGTA
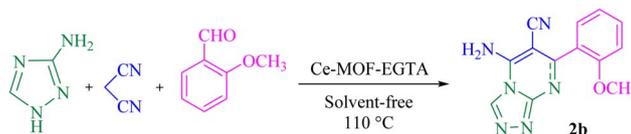
Entry	Condition	Catal. amount (mg)	Time (min)	Yield (%)
1	Solvent-free, 90 °C	20	30	79
2	**Solvent-free, 110°C**	**20**	**30**	**98**
3	Solvent-free, 130 °C	20	30	85
4	Solvent-free, 110 °C	10	30	75
5	Solvent-free, 110 °C	30	30	68
6	Solvent-free, 110 °C	20	20	82
7	Solvent-free, 110 °C	20	40	77
8	Solvent-free, 110 °C	20	60	65
9	Solvent-free, 110 °C	—	60	Trace
10	DMF, 110 °C	20	30	63
11	EtOH, reflux	20	30	70
12	CH₃CN, reflux	20	30	55
13	THF, reflux	20	30	60
14	Toluene, reflux	20	30	57
15	*n*-Hexane, reflux	20	30	50
16	H₂O, reflux	20	30	70
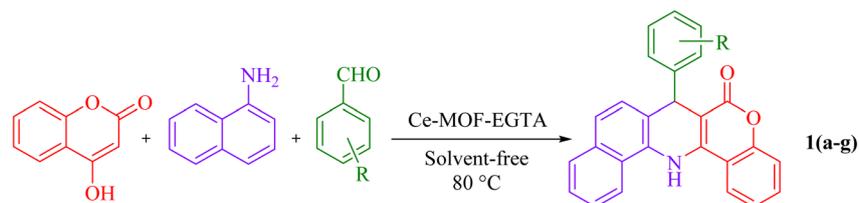
(C–H aliphatic), 1661 (C=O), 1472 (C=C aromatic) and 1268 (C–O). ^{1}H NMR (250 MHz, DMSO-d$_6$) δ = 9.45 (s, 1H, NH), 9.21 (s, 1H, OH), 8.61 (d, J = 8.4 Hz,1H, H aromatic), 8.56 (d, J = 8.0 Hz, 1H, H aromatic), 7.85 (d, J = 8.0 Hz, 1H, H aromatic), 7.68–7.56 (m, 2H, H aromatic), 7.53 (d, J = 7.3 Hz, 2H, H aromatic), 7.37 (q, J = 11.0 Hz, 3H, H aromatic), 6.98 (t, J = 7.8 Hz, 1H, H aromatic), 6.74 (d, J = 7.6 Hz, 1H, H aromatic), 6.66 (s,1H, H aromatic), 6.49 (d, J = 5.7 Hz, 1H, H aromatic), 5.26 (s, 1H, H aliphatic). ^{13}C NMR (62.5 MHz, DMSO-d$_6$) δ = 161.0 (C=O), 157.8, 152.7, 148.6, 144.3, 133.1, 132.3, 130.5, 129.7, 128.6, 127.8, 126.5, 126.4, 124.4, 124.2, 123.9, 123.2,

122.3, 121.0, 118.5, 117.2, 114.7, 114.1, 113.9, 99.1 (C aromatic), 41.9 (C aliphatic).

7-(2,3-Dihydroxyphenyl)-7,14-dihydro-6H-benzo[h]chromeno [4,3-b]quinolin-6-one (1e). Cream solid, M.P. 280–283 °C, IR (KBr, cm^{-1}): 3417 (NH), 2924 (C–H aromatic), 1647 (C=O), 1472 (C=C aromatic) and 1266 (C–O). ^{1}H NMR (250 MHz, DMSO-d$_6$) δ = 9.28 (d, J = 13.8 Hz, 2H, OH), 8.64–8.47 (m, 3H, H aromatic), 7.80 (d, J = 7.8 Hz, 1H, NH), 7.70–7.33 (m, 7H, H aromatic), 6.59–6.32 (m, 3H, H aromatic), 5.78 (s,1H, H aliphatic).

7-(2-Chlorophenyl)-7,14-dihydro-6H-benzo[h]chromeno[4,3-b] quinolin-6-one (1f). Cream solid, M.P. 335–337 °C, IR (KBr, cm^{-1}): 3327 (NH), 3065 (C–H aromatic), 1663 (C=O), 1619
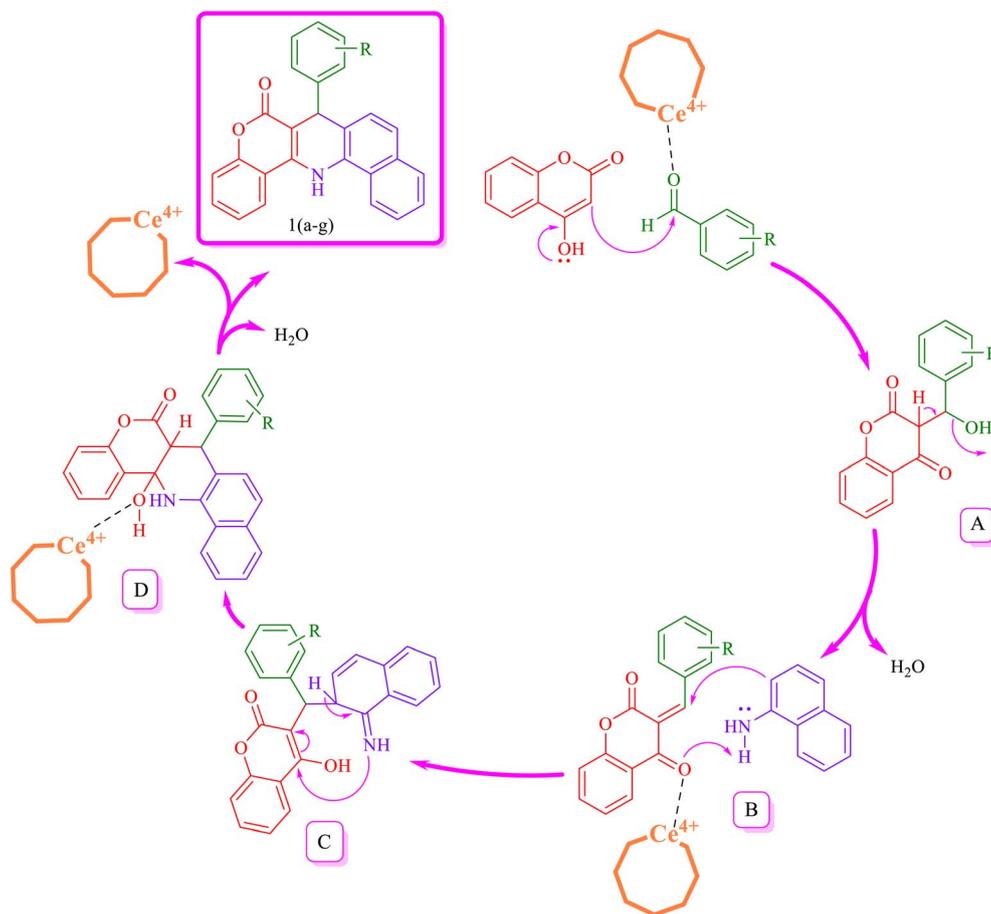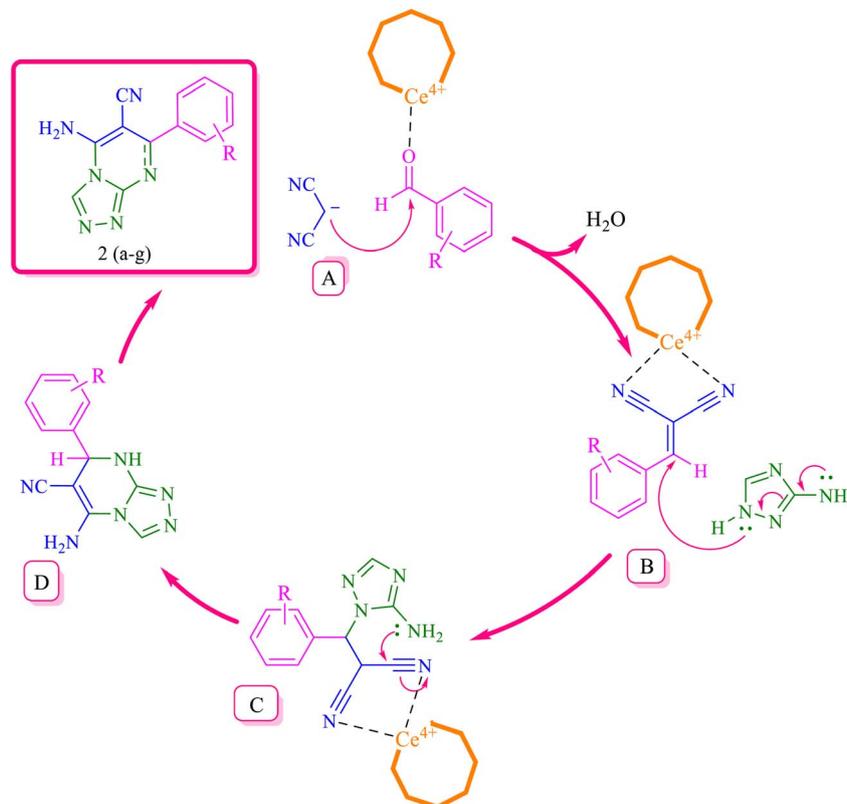

Fig. 10 Plausible mechanism for the synthesis of **1(a–g)** by Ce-MOF-EGTA.

Fig. 11 Plausible mechanism for the synthesis of **2(a–g)** by Ce-MOF-EGTA. Generally, the high catalytic efficiency observed for Ce-MOF-EGTA highlights the functional importance of its flexible framework. In this MOF, the aliphatic tetratopic EGTA ligand coordinates to Ce centers through its four binding sites, forming a stable yet flexible network. This coordination arrangement allows the ligand to adopt different conformations, creating an adaptive pore environment that facilitates substrate diffusion and proper alignment of reactants near the Lewis acidic Ce sites. The flexible nature of the ligand framework enables the MOF to accommodate substrates of varying sizes and shapes, consistent with a breathing or conformational flexibility observed in other flexible MOFs.[55,56]

(NH bend), 1471 (C=C aromatic) and 1272 (C–O). ^{1}H NMR (250 MHz, DMSO-d$_6$) δ = 9.38 (s, 1H, NH), 8.57 (dd, J = 13.2, 8.3 Hz, 2H, H aromatic), 7.81 (d, J = 8.1 Hz, 1H, H aromatic), 7.65 (d, J = 8.6 Hz, 2H, H aromatic), 7.51 (dd, J = 11.7, 7.8 Hz, 4H, H aromatic), 7.37 (d, J = 8.1 Hz, 2H, H aromatic), 7.29 (d, J = 8.6 Hz,1H, H aromatic), 7.16–7.10 (m, 2H, H aromatic), 5.88 (s, 1H, H aliphatic).
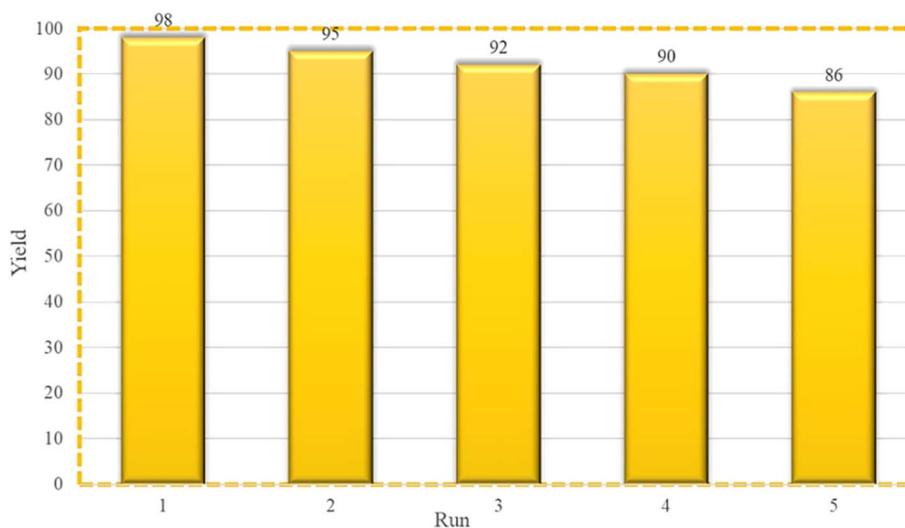
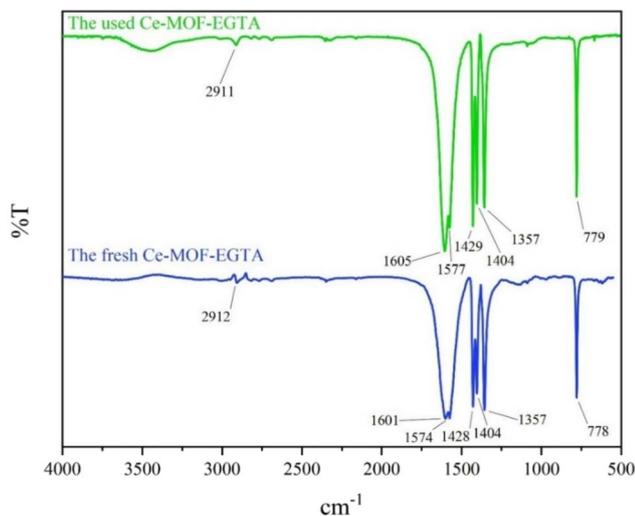**Fig. 12** Recyclability of the Ce-MOF-EGTA catalyst.

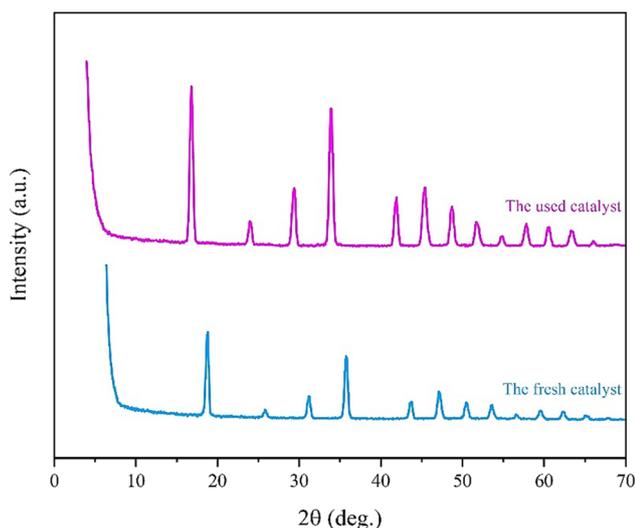Fig. 13   The FT-IR spectra of fresh Ce-MOF-EGTA and used Ce-MOF-EGTA.

Fig. 14   The XRD pattern of the used and fresh Ce-MOF-EGTA.

7-(4-Methoxyphenyl)-7,14-dihydro-6H-benzo[h]chromeno[4,3-b] quinolin-6-one (1g). Yellow solid, M.P. 330–333 °C, IR (KBr, cm^{-1}): 3295 (NH), 2992 (C–H aromatic), 1665 (C=O), 1622

(NH bend), 1400 (C=C aromatic) and 1246 (C–O). ^{1}H NMR (250 MHz, DMSO-d$_6$) δ = 9.44 (s, 1H, NH), 8.58 (dd, J = 18.4, 8.2 Hz,2H, H aromatic), 7.84 (d, J = 7.9 Hz, 1H, H aromatic), 7.69–7.28 (m, 7H, H aromatic), 7.17 (d, J = 8.2 Hz, 2H, H aromatic), 6.74 (d, J = 8.2 Hz, 2H, H aromatic), 5.29 (s,1H, H aliphatic), 3.61 (s, 3H, OCH$_3$).

5-Amino-7-phenyl-7,8-dihydro-[1,2,4]triazolo[4,3-a]pyrimidine-6-carbonitrile (2a). Yellow solid, M.P. 259–262 °C, IR (KBr, cm^{-1}): 3357 (NH$_2$), 3267 (NH), 3183 (C–H aromatic), 2190 (C≡N), 1531 (C=N) and 1367 (C=C aromatic). ^{1}H NMR (300 MHz, DMSO-d$_6$) δ = 8.80 (s, 1H, NH), 7.74 (s, 1H, H aromatic), 7.48–7.35 (m, 2H, NH$_2$), 7.32 (ddd, J = 8.2, 6.6, 1.6 Hz, 3H, H aromatic), 7.24 (s, 2H, H aromatic), 5.37 (d, J = 2.0 Hz, 1H, H aliphatic). ^{13}C NMR (75 MHz, DMSO-d$_6$) δ = 160.5, 158.3, 157.6, 156.4, 154.8, 154.5, 152.4, 147.5, 143.7, 135.7, 131.0, 130.2, 129.2, 128.5, 128.3, 126.5 (C aromatic), 119.5 (CN), 56.5 (C aliphatic).

5-Amino-7-(2-methoxyphenyl)-7,8-dihydro-[1,2,4]triazolo[4,3-a] pyrimidine-6-carbonitrile (2b). Yellow solid, M.P. 252–255 °C, IR (KBr, cm^{-1}): 3456 (NH$_2$), 3360 (NH), 3265 (C–H aromatic), 3008 (C–H aliphatic), 2189 (C≡N), 1630 (C=N) and 1485 (C=C aromatic), 1236 (C–O). ^{1}H NMR (500 MHz,DMSO-d$_6$) δ = 8.41 (d, J = 2.5 Hz, 1H, NH), 7.66 (s, 1H, H aromatic), 7.30–7.26 (m, 1H, H aromatic), 7.10 (dd, J = 7.5, 1.7 Hz, 1H, H aromatic), 7.06 (s, 2H, NH$_2$), 7.02 (d, J = 8.2 Hz, 1H, H aromatic), 6.91 (t, J = 7.4 Hz, 1H, H aromatic), 5.45 (d, J = 2.5 Hz, 1H, H aliphatic), 3.68 (s, 3H, OCH$_3$). ^{13}C NMR (125 MHz, DMSO-d$_6$) δ = 157.1, 154.7, 152.0, 147.8, 131.0, 129.8, 127.5, 120.8, 119.4 (C aromatic), 112.0 (CN), 55.9 (C aliphatic), 55.5 (OCH$_3$).

5-Amino-7-(3,4-dimethoxyphenyl)-7,8-dihydro-[1,2,4]triazolo [4,3-a]pyrimidine-6-carbonitrile (2c). Yellow solid, M.P. 284–288 °C, IR (KBr, cm^{-1}): 3323 (NH$_2$), 3196 (C–H aromatic), 2963 (C–H aliphatic), 2219 (C≡N), 1682 (C=N) and 1466 (C=C aromatic). ^{1}H NMR (500 MHz, DMSO-d$_6$) δ = 8.96 (s, 2H, NH$_2$), 8.36–8.33 (m, 1H, H aromatic), 7.24 (d, J = 15.8 Hz, 2H, H aromatic), 6.89 (s, 1H, H aromatic), 3.61 (s, 3H, OCH$_3$), 3.10 (s, 3H, OCH$_3$). ^{13}C NMR (125 MHz, DMSO-d$_6$) δ = 164.1, 156.4, 155.5, 152.1, 151.4, 148.7, 129.5, 122.5, 116.4, 112.6, 111.6 (C aromatic),75.5 (CN), 56.1 (OCH$_3$).

5-Amino-7-(4-chlorophenyl)-[1,2,4]triazolo[4,3-a]pyrimidine-6-carbonitrile (2d). White solid, M.P. 295–300 °C, IR (KBr, cm^{-1}): 3351 (NH$_2$), 3056 (C–H aromatic), 2197 (C≡N), 1661 (C=N), 1593 (NH$_2$ in plan bend), 1485 (C=C aromatic) and 1157 (C–N).
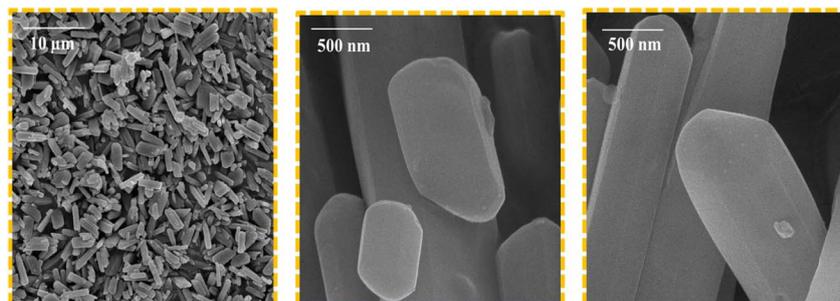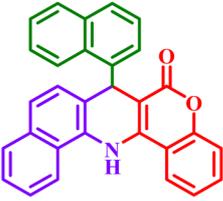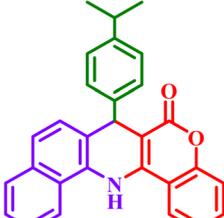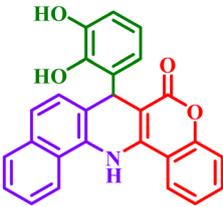

Fig. 15   FESEM images of Ce-MOF-EGTA.

**Table 4** Synthesis of **1(a–g)** and **2(a–g)** by Ce-MOF-EGTA

1a
M.P. (°C) = >350 (no clear melt)
Time (min) = 12
Yield (%) = 91
[a]TON = 0.155 × 10⁴
[b]TOF = 0.778 × 10⁴ h⁻¹

1b
M.P. (°C) = >300 (decompose)
Time (min) = 10
Yield (%) = 97
TON = 0.165 × 10⁴
TOF = 0.995 × 10⁴ h⁻¹

1c
M.P. (°C) = 305-307
Time (min) = 12
Yield (%) = 93
TON = 0.158 × 10⁴
TOF = 0.795 × 10⁴ h⁻¹

1d
M.P. (°C) = 336-339
Time (min) = 10
Yield (%) = 95
TON = 0.162 × 10⁴
TOF = 0.975 × 10⁴ h⁻¹

1e
M.P. (°C) = 280-283
Time (min) = 12
Yield (%) =82
TON = 0.140 × 10⁴
TOF = 0.701 × 10⁴ h⁻¹
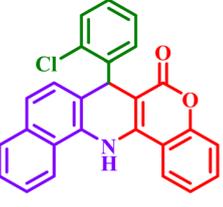
1f
M.P. (°C) = 335-337
Time (min) = 15
Yield (%) = 90
TON = 0.153 × 10⁴
TOF = 0.615 × 10⁴ h⁻¹

1g
M.P. (°C) = 330-333
Time (min) = 12
Yield (%) = 88
TON = 0.150 × 10⁴
TOF = 0.752 × 10⁴ h⁻¹

2a
M.P. (°C) = 260-265
Time (min) = 25
Yield (%) =86
TON = 0.147 × 10⁴
TOF = 0.353 × 10⁴ h⁻¹

2b
M.P. (°C) = 252-255
Time (min) = 30
Yield (%) = 98
TON = 0.168 × 10⁴
TOF = 0.335 × 10⁴ h⁻¹

2c
M.P. (°C) = 284-288
Time (min) = 30
Yield (%) = 92
TON = 0.157 × 10⁴
TOF = 0.315 × 10⁴ h⁻¹
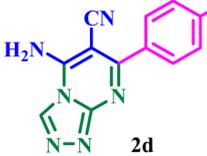
2d
M.P. (°C) = 295-300
Time (min) = 35
Yield (%) = 93
TON = 0.159 × 10⁴
TOF = 0.273 × 10⁴ h⁻¹

2e
M.P. (°C) = 280-285
Time (min) = 35
Yield (%) = 89
TON = 0.152 × 10⁴
TOF = 0.261 × 10⁴ h⁻¹

2f
M.P. (°C) = >300 (decmpose)
Time (min) = 35
Yield (%) = 85
TON = 0.145 × 10⁴
TOF = 0.249 × 10⁴ h⁻¹

2g
M.P. (°C) = 270-275
Time (min) = 30
Yield (%) = 91
TON = 0.156 × 10⁴
TOF = 0.311 × 10⁴ h⁻¹

[a] TON (turnover number) = Moles of desired product formed/moles of catalyst. [b] TOF (turnover frequency) = Turnover number (TON)/minutes.

¹H NMR (250 MHz, DMSO-d₆) δ = 9.30 (s, 2H, NH₂), 8.61 (s, 1H, H aromatic), 7.85 (d, J = 8.2 Hz, 2H, H aromatic), 7.64 (d, J = 8.4 Hz, 2H, H aromatic). ¹³C NMR (62.5 MHz, DMSO-d₆) δ = 156.4, 151.9, 136.2, 131.0, 128.9 (C aromatic), 115.9 (CN).

5-Amino-7-(4-fluorophenyl)-7,8-dihydro-[1,2,4]triazolo[4,3-a] pyrimidine-6-carbonitrile (2e). White solid, M.P. 280–285 °C, IR (KBr, cm⁻¹): 3351 (NH₂), 3238 (NH), 3114 (C–H aromatic), 2195 (C≡N), 1661 (C=N) and 1485 (C=C aromatic). ¹H NMR (300
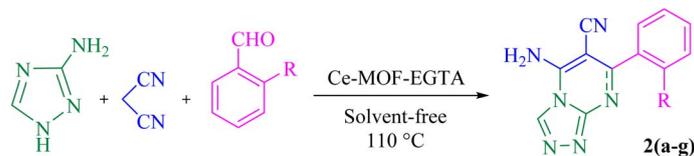
MHz, DMSO-d_6) δ = 8.97 (s, 1H, NH), 8.30–8.27 (m, 2H, NH$_2$), 7.77 (s, 1H, H aromatic), 7.60 (d, J = 8.8 Hz, 2H, H aromatic), 7.38 (s, 2H, H aromatic), 5.60 (s, 1H, H aliphatic).

5-Amino-7-(pyridin-3-yl)-[1,2,4]triazolo[4,3-a]pyrimidine-6-carbonitrile (2f). Light brown solid, M.P. > 300 °C, IR (KBr, cm^{-1}): 3434 (NH$_2$), 2928 (C–H aromatic), 2190 (C≡N), 1684 (C=N), 1537 (C=C aromatic) and 1580 (NH$_2$ in plane bend). ^{1}H NMR (250 MHz, DMSO-d_6) δ = 9.37 (s, 2H, NH$_2$), 8.97 (s, 1H, H aromatic), 8.67 (d, J = 27.8 Hz, 2H, H aromatic), 8.21 (d, J = 7.8 Hz, 1H, H aromatic), 7.60 (s, 1H, H aromatic).

5-Amino-7-(p-tolyl)-7,8-dihydro-[1,2,4]triazolo[4,3-a]pyrimidine-6-carbonitrile (2g). White solid, M.P. 270–275 °C, IR (KBr, cm^{-1}): 3349 (NH$_2$), 3263 (NH), 3187 (C–H aromatic), 3118 (C–H aliphatic), 2194 (C≡N), 1661 (C=N) and 1530 (C=C aromatic). ^{1}H NMR (250 MHz, DMSO-d_6) δ = 9.21 (s, 1H, NH), 8.63 (d, J = 32.0 Hz, 2H, NH$_2$), 7.75–7.64 (m, 1H, H aromatic), 7.15 (s, 5H, H aromatic), 5.25 (s, 1H, H aromatic), 2.26 (d, J = 30.9 Hz, 3H, CH$_3$).

Proposed mechanism for the synthesis of 1(a–g) and 2(a–g). Proposed mechanism for the synthesis of **1(a–g)** is shown in Fig. 10. The Ce-MOF-EGTA catalyst facilitates the reaction by providing accessible Ce Lewis acid sites, which coordinate to the carbonyl group of the aldehyde, increasing its electrophilicity. The condensation between 4-hydroxycoumarine and the activated aldehyde gives the intermediate **A**, which subsequently loses H$_2$O, to afford the intermediate **B**. Afterward, a nucleophilic attack of 1-naphthylamine to the activated intermediate **B** gives the intermediate **C**, which readily undergoes a subsequent intramolecular cyclization to produce the intermediate **D**. Finally, the dehydration of intermediate **D** affords the target molecule **1(a–g)**. Additionally, the flexible framework of the EGTA ligand facilitate substrate diffusion and proper orientation, enhancing the reaction efficiency and contributing to the observed high yields under mild conditions.

The proposed mechanism for the synthesis of **2(a–g)** is shown in Fig. 11. The aldehyde is activated by the Ce Lewis acid sites of Ce-MOF-EGTA, which increases its electrophilicity and facilitates the initial condensation with malononitrile to form the benzylidene intermediate **A**. Intermediate **A** then undergoes a Michael addition with 3-amino-1,2,4-triazole, generating intermediate **B**. Subsequent intramolecular cyclization of intermediate **B** affords the expected cyclic products. Anomeric-based oxidation or air-oxidation leads to hydride transfer, controlling the ring aromaticity. In this reaction as well, the structural arrangement of the ligand can assist in aligning the reactants within the framework.

Reusability of the Ce-MOF-EGTA. In a separate study, we studied the easy recyclability of this catalyst for the synthesis of target molecule 7-(2-methoxyphenyl)-7,14-dihydro-6H-benzo[h]chromeno[4,3-b]quinolin-6-one **1b** and 5-amino-7-(2-methoxy-phenyl)-7,8-dihydro-[1,2,4]triazolo[4,3-a]pyrimidine-6-carbonitrile **2b** under optimal reaction conditions. At the end of each run, the solid was dissolved in 10 mL of DMF and centrifuged to separate the Ce-MOF-EGTA catalyst. The separated catalyst was washed with DMF and EtOH, dried, and reused for the next run. The results indicated that Ce-MOF-EGTA could be reused 5 times without any considerable decrease in the reaction yield (Fig. 12).

Moreover, the used catalyst was evaluated after the fifth catalytic cycle by the FT-IR, XRD, and FESEM techniques. As shown in Fig. 13, the IR index peaks of the synthesized framework were preserved in the recycled catalyst, which indicates the stability of the recycled catalyst.

On the other hand, the XRD spectrum of the used Ce-MOF-EGTA catalyst shows that the crystalline phase is preserved (Fig. 14).

In addition, the SEM images reveal that the catalyst's structure remains intact (Fig. 15).

According to the structural analysis (FT-IR, XRD and SEM), the recovered catalyst retains its original structure, indicating negligible Ce leaching. Moreover, a hot filtration test was performed: the catalyst was removed from the reaction mixture midway, and the reaction continued without noticeable change in rate or yield, suggesting minimal Ce leaching. We have not performed ICP or EDX analysis to quantitatively measure leaching; however, based on the hot filtration test, any leaching is expected to be very low.

Conclusion

A novel cerium-based flexible MOF (Ce-MOF-EGTA) constructed from an aliphatic tetratopic ligand was developed as an efficient and reusable heterogeneous catalyst. EGTA introduces intrinsic conformational flexibility due to its aliphatic backbone and chelating ether groups, leading to an adaptive framework. Moreover, Ce provides accessible Lewis acid sites, which are rarely explored in flexible MOFs for catalytic applications. Its intrinsic framework flexibility combined with accessible Ce Lewis acid sites enables high-yield synthesis of biologically relevant heterocycles under mild and green conditions. The catalyst retains its structure and activity over multiple cycles, demonstrating excellent stability and recyclability. This study

highlights the potential of aliphatic-ligand-based flexible MOFs for sustainable and adaptive catalytic applications, opening avenues for future design of functional MOFs.

Conflicts of interest

There is no conflicts to declare.

Data availability

All data generated or analyzed during this study are included in the Main manuscript text.

References

1 V. Mishra and A. Mishra, Introduction of metal-organic frameworks (MOFs), in *Metal–Organic Frameworks as Forensic Detectors*, Springer Nature Singapore, Singapore, 2025, pp. 1–20.

2 V. F. Yusuf, N. I. Malek and S. K. Kailasa, Review on metal–organic framework classification, synthetic approaches, and influencing factors: applications in energy, drug delivery, and wastewater treatment, *ACS Omega*, 2022, **7**, 44507–44531.

3 M. Rubio-Martinez, C. Avci-Camur, A. W. Thornton, I. Imaz, D. Maspoch and M. R. Hill, New synthetic routes towards MOF production at scale, *Chem. Soc. Rev.*, 2017, **46**, 3453–3480.

4 Z. Han, Y. Yang, J. Rushlow, J. Huo, Z. Liu, Y. C. Hsu, R. Yin, M. Wang, R. Liang, K. Y. Wang and H. C. Zhou, Development of the design and synthesis of metal–organic frameworks (MOFs)–from large scale attempts, functional oriented modifications, to artificial intelligence (AI) predictions, *Chem. Soc. Rev.*, 2025, **54**, 367–395.

5 H. Laeim, V. Molahalli, P. Prajongthat, A. Pattanaporkratana, G. Pathak, B. Phettong, N. Hongkarnjanakul and N. Chattham, Porosity tunable metal-organic framework (MOF)-based composites for energy storage applications: recent progress, *Polymers*, 2025, **17**, 130.

6 C. Liu, C. Tian, J. Guo, X. Zhang, L. Wu, L. Zhu and B. Du, Research progress of metal organic frameworks as drug delivery systems, *ACS Appl. Mater. Interfaces*, 2024, **16**, 43156–43170.

7 A. Ali, J. M. Moradian, A. Naveed, S. Zhang, M. H. Tahir, K. Shehzad and M. Sillanpää, Progress in cathode materials for rechargeable zinc-ion batteries: from inorganic and organic systems to hybrid frameworks and biomass-derived innovations, *Prog. Mater. Sci.*, 2025, 101543.

8 S. Essalmi, S. Lotfi, A. BaQais, M. Saadi, M. Arab and H. A. Ahsaine, Design, and application of metal organic frameworks for heavy metals adsorption in water: a review, *RSC Adv.*, 2024, **14**, 9365–9390.

9 G. R. Xu, Z. H. An, K. Xu, Q. Liu, R. Das and H. L. Zhao, Metal organic framework (MOF)-based micro/nanoscaled materials for heavy metal ions removal: the cutting-edge study on designs, synthesis, and applications, *Coord. Chem. Rev.*, 2021, **427**, 213554.

10 D. Wang, H. Yao, J. Ye, Y. Gao, H. Cong and B. Yu, Metal organic frameworks (MOFs): classification, synthesis, modification, and biomedical applications, *Small*, 2024, **20**, 2404350.

11 S. Kumar, S. Jain, M. Nehra, N. Dilbaghi, G. Marrazza and K. H. Kim, Green synthesis of metal organic frameworks: a state-of-the-art review of potential environmental and medical applications, *Coord. Chem. Rev.*, 2020, **420**, 213407.

12 P. S. Sharanyakanth and M. Radhakrishnan, Synthesis of metal-organic frameworks (MOFs) and its application in food packaging: a critical review, *Trends Food Sci. Technol.*, 2020, **104**, 102–116.

13 S. Yadav, R. Dixit, S. Sharma, S. Dutta, K. Solanki and R. K. Sharma, Magnetic metal organic framework composites: structurally advanced catalytic materials for organic trans-formations, *Mater. Adv.*, 2021, **2**, 2153–2187.

14 H. Ghasempour, K. Y. Wang, J. A. Powell, F. Zare Karizi, X. L. Lv, A. Morsali and H. C. Zhou, Metal–organic frameworks based on multicarboxylate linkers, *Coord. Chem. Rev.*, 2021, **426**, 213542.

15 D. Yang, Y. Chen, Z. Su, X. Zhang, W. Zhang and K. Srinivas, Organic carboxylate-based MOFs and derivatives for electrocatalytic water oxidation, *Coord. Chem. Rev.*, 2021, **428**, 213619.

16 A. V. Desai, S. Sharma, S. Let and S. K. Ghosh, *N*-donor linker-based metal-organic frame-works (MOFs): advancement and prospects as functional materials, *Coord. Chem. Rev.*, 2019, **395**, 146–192.

17 J. H. Lee, S. Jeoung, Y. G. Chung and H. R. Moon, Elucidation of flexible metal-organic frameworks: research progresses and recent developments, *Coord. Chem. Rev.*, 2019, **389**, 161–188.

18 J. Kaur and G. Kaur, Review on flexible metal-organic frameworks, *Mater. Adv.*, 2021, **6**, 8227–8243.

19 J. Chen, Q. Zhang, J. Dong, F. Xu and S. Li, Amino-functionalized Cu metal organic framework nanosheets as fluorescent probes for detecting TNP, *Anal. Methods*, 2021, **13**, 5328–5334.

20 M. A. Farajzadeh, S. Rahimzadeh, M. R. A. Mogaddam and M. B. Aghdam, A fast and simple procedure for the synthesis of a zinc and 1,4-benzene dicarboxylic acid metal–organic framework and its evaluation as a sorbent for dispersive micro solid phase extraction of pesticide residues, *RSC Adv.*, 2024, **14**, 28035–28043.

21 R. Darabi and H. Karimi-Maleh, Hierarchical copper-1,3,5-benzene-tricarboxylic acid-MOF-derived with nitrogen-doped graphene nanoribbons as a novel assembly nanocomposite for asymmetric supercapacitors, *Adv. Compos. Hybrid Mater.*, 2023, **6**, 114.

22 N. Kumar Sundarraj, J. Q. S. Pandiyan, A. Al Souwaileh, J. J. Wu and S. Anandan, Sono-chemical synthesis of Ni-MOF using 2-methylimidazole as an organic linker: pushing the boundaries of energy storage, *Electrochim. Acta*, 2025, **523**, 145975.

23 L. Biswal, J. E. Goodwill, C. Janiak and S. Chatterjee, Versatility, cost analysis, and scale-up in fluoride and

arsenic removal using metal-organic framework-based adsorbents, *Sep. Purif. Rev.*, 2022, **51**, 408–426.

24 H. Li, Q. Li, X. He, N. Zhang, Z. Xu and Y. Wang, The magnetic hybrid Cu(I)-MOF@Fe₃O₄ with hierarchically engineered micropores for highly efficient removal of Cr(VI) from aqueous solution, *Cryst. Growth Des.*, 2018, **18**, 6248–6256.

25 P. A. Demakov, Properties of aliphatic ligand-based metal organic frameworks, *Polymers*, 2023, **15**, 2891.

26 Z. J. Lin, J. Lü, M. Hong and R. Cao, Metal organic frameworks based on flexible ligands (FL-MOFs): structures and applications, *Chem. Soc. Rev.*, 2014, **43**, 5867–5895.

27 M. Chang, Y. Zhao, D. Liu, J. Yang, J. Li and C. Zhong, Methane-trapping metal organic frameworks with an aliphatic ligand for efficient CH_4/N_2 separation, *Sustain. Energy Fuels*, 2020, **4**, 138–142.

28 D. H. Hong and M. P. Suh, Enhancing CO_2 separation ability of a metal organic framework by post-synthetic ligand exchange with flexible aliphatic carboxylates, *Chem. Eur. J.*, 2014, **20**, 426–434.

29 G. Férey and C. Serre, Large breathing effects in three-dimensional porous hybrid matter: facts, analyses, rules and consequences, *Chem. Soc. Rev.*, 2009, **38**, 1380–1399.

30 P. A. Demakov, A. S. Poryvaev, K. A. Kovalenko, D. G. Samsonenko, M. V. Fedin, V. P. Fedin and D. N. Dybtsev, Structural dynamics and adsorption properties of the breathing microporous aliphatic metal organic framework, *Inorg. Chem.*, 2020, **59**, 15724–15732.

31 G. Férey, A selective magnetic sponge, *Nat. Mater.*, 2003, **2**, 136–137.

32 D. Maspoch, D. Ruiz-Molina, K. Wurst, N. Domingo, M. Cavallini, F. Biscarini, J. Tejada, C. Rovira and J. Veciana, A nanoporous molecular magnet with reversible solvent-induced mechanical and magnetic properties, *Nat. Mater.*, 2003, **2**, 190–195.

33 N. Zigon, V. Duplan, N. Wada and M. Fujita, Crystalline sponge method: X-ray structure analysis of small molecules by post-orientation within porous crystals-principle and proof-of-concept studies, *Angew. Chem., Int. Ed.*, 2021, **60**, 25204–25222.

34 G. Alberti, S. Murcia-Mascaros and R. Vivani, Pillared derivatives of γ-zirconium phosphate containing nonrigid alkyl chain pillars, *J. Am. Chem. Soc.*, 1998, **120**, 9291–9295.

35 T. K. Kim, K. J. Lee, M. Choi, N. Park, D. Moon and H. R. Moon, Metal–organic frameworks constructed from flexible ditopic ligands: conformational diversity of an aliphatic ligand, *New J. Chem.*, 2013, **37**, 4130–4139.

36 H. Reinsch, R. S. Pillai, R. Siegel, J. Senker, A. Lieb, G. Maurin and N. Stock, Structure and properties of Al-MIL-53-ADP, a breathing MOF based on the aliphatic linker molecule adipic acid, *Dalton Trans.*, 2016, **45**, 4179–4186.

37 H. Reinsch, T. Homburg, N. Heidenreich, D. Fröhlich, S. Hennninger, M. Wark and N. Stock, Green synthesis of a new Al-MOF based on the aliphatic linker mesaconic acid: structure, properties and *in situ* crystallization studies of Al-MIL-68-Mes, *Chem. Eur. J.*, 2018, **24**, 2173–2181.

38 V. D. Slyusarchuk, P. E. Kruger and C. S. Hawes, Cyclic aliphatic hydrocarbons as linkers in metal-organic frameworks: new frontiers for ligand design, *ChemPlusChem*, 2020, **85**, 845–854.

39 K. D. Abasheeva, P. A. Demakov, E. V. Polyakova, A. N. Lavrov, V. P. Fedin and D. N. Dybtsev, Synthesis, structural versatility, magnetic properties, and (I) adsorption in a series of cobalt(II) metal–organic frameworks with a charge-neutral aliphatic (O, O)-donor bridge, *Nanomater.*, 2023, **13**, 2773.

40 P. A. Demakov, A. S. Poryvaev, K. A Kovalenko, D. G. Samsonenko, M. V. Fedin, V. P. Fedin and D. N. Dybtsev, Structural dynamics and adsorption properties of the breathing microporous aliphatic metal–organic framework, *Inorg. Chem.*, 2020, **59**, 15724–15732.

41 J. Wang, Y. C. Ou, Y. Shen, L. Yun, J. D. Leng, Z. Lin and M. L Tong, Coordination chemistry of cyclohexane-1,2,4,5-tetracarboxylate (H₄L). Synthesis, structure, and magnetic properties of metal-organic frameworks with conformation-flexible H₄L ligand, *Cryst. Growth Des.*, 2009, **9**, 2442–2450.

42 M. Beiranvand, D. Habibi and H. Khodakarami, Novel UiO-NH₂-like Zr-based MOF (Basu-DPU) as an excellent catalyst for preparation of new 6*H*-chromeno[4,3-*b*]quinolin-6-ones, *ACS Omega*, 2023, **8**, 25924–25937.

43 P. Sanati-Tirgan and H. Eshghi, Synthesis, characterization, and application of MOF/COF hybrid composite as a highly active and recyclable catalyst for multicomponent synthesis of chromeno[4,3-*b*]quinoline-6-ones, *Appl. Organomet. Chem.*, 2025, **39**, e70039.

44 G. Rahimzadeh, S. Bahadorikhalili, E. Kianmehr and M. Mahdavi, Ionic liquid-functionalized magnetic nanostructures as an efficient catalyst for the synthesis of 6*H*-chromeno[4,3-*b*] quinolin-6-ones, *Mol. Divers.*, 2017, **21**, 597–609.

45 R. Singha, A. Islam and P. Ghosh, One-pot three-component tandem annulation of 4-hydroxy-coumarine with aldehyde and aromatic amines using graphene oxide as an efficient catalyst, *Sci. Rep.*, 2021, **11**, 19891.

46 Z. Chen, J. Bi and W. Su, Synthesis, and antitumor activity of novel coumarin derivatives *via* a three-component reaction in water, *Chin. J. Chem.*, 2013, **31**, 507–514.

47 A. Benrashid, D. Habibi and M. Beiranvand, Deep eutectic solvent-immobilized magnetic nanoparticles as a capable catalyst for the green synthesis of triazolopyrimidines, *J. Mol. Liq.*, 2024, **409**, 125504.

48 M. Lashkari, M. Ghashang and A. Abedi-Madiseh, Soluble glass, an efficient promoter for the cascade addition-cyclization reaction of 4-hydroxycoumarins to chalcone derivatives, *Org. Prep. Proced. Int.*, 2020, **53**, 52–58.

49 A. Dandia, P. Sarawgi, K. Arya and S. Khaturia, Mild and ecofriendly tandem synthesis of 1, 2,4-triazolo[4,3-*a*] pyrimidines in aqueous medium, *Arkivoc*, 2006, **16**, 83–92.

50 N. Jamasbi, M. Irankhah-Khanghah, F. Shirini, H. Tajik and M. S. N. Langarudi, DABCO-based ionic liquids:

introduction of two metal-free catalysts for one-pot synthesis of 1,2,4-triazolo[4,3-*a*]pyrimidines and pyrido[2,3-*d*] pyrimidines, *New J. Chem.*, 2018, **42**, 9016–9027.

51 S. S. Pandit, S. K. Bhalerao, U. S. Aher, G. L. Adhav and V. U. Pandit, Amberlyst A-15: reusable catalyst for the synthesis of 2,4,5-trisubstituted and 1,2,4,5-tetrasubstituted-1*H*-imidazoles under MW irradiation, *J. Chem. Sci.*, 2011, **123**, 421–426.

52 P. Chhattise, S. Saleh, V. Pandit, S. Arbuj and V. Chabukswar, ZnO nanostructures: a heterogeneous catalyst for the synthesis of benzoxanthene and pyranopyrazole scaffolds *via* a multi-component reaction strategy, *Mater. Adv.*, 2020, **1**, 2339–2345.

53 S. Pandit, R. Shaikh and V. Pandit, Synthesis of 5-unsubstituted-3,4-dihydropyridine-2-(1*H*)-ones using nbs as a catalyst under solvent free conditions, *Rasayan J. Chem.*, 2009, **2**, 907–911.

54 X. Wang, Y. Zhang, Z. Shi, T. Lu, Q. Wang and B. Li, Multifunctional Zr-MOF based on bisimidazole tetracarboxylic acid for pH sensing and photoreduction of Cr(VI), *ACS Appl. Mater. Interfaces*, 2021, **13**, 54.

55 A. Dhakshinamoorthy and H. Garcia, Metal–organic frameworks as solid catalysts for the synthesis of nitrogen-containing heterocycles, *Chem. Soc. Rev.*, 2014, **43**, 5750–5765.

56 P. A. Demakov, Properties of aliphatic ligand-based metal–organic frameworks, *Polymers*, 2023, **15**, 2891.